Journal of Catalysis 413 (2022) 93–105

Contents lists available at ScienceDirect

Journal of Catalysis

journal homepage: www.elsevier.com/locate/jcat

Tailoring single site VO_4 on flame-made V/Al_2O_3 catalysts for selective oxidation of *n*-butane

Zichun Wang [a,b], Yijiao Jiang [b], Wenjie Yang [a], Ang Li [c], Michael Hunger [d,*], Alfons Baiker [e,*], Jun Huang [a,*]

[a] Laboratory for Catalysis Engineering, School of Chemical and Biomolecular Engineering & Sydney Nano Institute, The University of Sydney, Sydney, NSW 2006, Australia
[b] Department of Engineering, Macquarie University, Sydney, New South Wales 2109, Australia
[c] Beijing Key Laboratory of Microstructure and Property of Advanced Materials, Beijing University of Technology, Beijing 100024, China
[d] Institute of Chemical Technology, University of Stuttgart, 70550 Stuttgart, Germany
[e] Institute for Chemical and Bioengineering, Department of Chemistry and Applied Biosciences, ETH Zürich, HCI, CH-8093 Zürich, Switzerland

ARTICLE INFO

Article history:
Received 4 March 2022
Revised 31 May 2022
Accepted 8 June 2022
Available online 13 June 2022

Keywords:
Solid-state NMR
Selective *n*-butane oxidation
Maleic anhydride
Vanadium oxide
Single-site VO_x

ABSTRACT

Selective aerobic oxidation of *n*-butane is one of the most complex selective aerobic oxidation reactions but is of great importance in producing maleic anhydride (MA) as a versatile chemical intermediate/platform in the chemical industry. Supported VO_x catalysts are extensively used in the selective oxidation of alkanes. However, the identification of active sites is quite challenging since various VO_x structures (single sites, clusters, nanoparticles, and crystals) and the related surface functional groups (V = O, V-O-V, and V-OH) can be formed on the surface. By simply tuning the V/Al ratios of V/Al_2O_3 catalysts, we prepared various VO_x structures using flame-spray pyrolysis and investigated their activities in the selective oxidation of *n*-butane to MA. The presence of single-site VO_x (SSV), polymeric VO_4 species, crystalline $AlVO_4$ clusters, and vanadium oxide is probed by systematic studies using ^{51}V and ^{27}Al solid-state NMR spectroscopy and confirmed by XRD, HRTEM, Raman, and UV–vis spectroscopies. VO_x single-sites interacting with surface penta-coordinated Al (Al^V) sites are identified as active sites promoting the conversion of *n*-butane to MA. V/Al_2O_3 with a high population of SSV-Al^V pairs in the amorphous Al_2O_3 network provides the best performance compared to other V/Al_2O_3 catalysts and those reported in the literature. Finally, a reaction mechanism based on the concerted action of SSV-Al^V pairs is proposed.
© 2022 Published by Elsevier Inc.

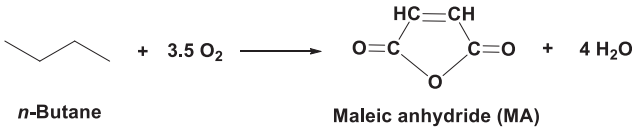
1. Introduction

Maleic anhydride (MA) is a versatile chemical intermediate/platform to produce key organic compounds (e.g. 1,4-butandiol), resins, coatings, lubricants, plasticizers, copolymers, and agricultural chemicals [1]. The global production of MA is about 3 million tons per year and increasing by 3–6 % annually [2,3]. In the first half of the 20th century, MA was mainly produced from the oxidation of benzene using supported VO_x and MoO_x catalysts, which suffers from atom inefficiency by the elimination of two carbon atoms, resulting in carbon dioxide emission. In the mid-1960 s, the selective aerobic oxidation of *n*-butane to MA using a vanadium pyrophosphate (VPO) catalyst was discovered by Bergman and Frisch [4]. The latter process is non-toxic, more economical and environmentally friendly, and accounts for ca. 80% MA production worldwide [1].

The selective aerobic oxidation of *n*-butane to MA is one of the most complex selective aerobic oxidation reactions [5–10]. In a single catalytic turnover, 14 electrons must be transferred to the catalyst surface from the substrate and three oxygen atoms must be inserted into the final molecule as shown in Scheme 1. The synthesis of MA often requires the concerted action of multifunctional groups (e.g. acid sites, V^{5+}/V^{4+} redox couple, V = O, V-O-V, V-O-P, and P = O) or lattice oxygen to promote the reaction on VPO catalysts [6,8,9,11]. It has been proposed that isolated VO_x species generated from the hydrolysis of surface δ-$VOPO_4$-like phases are possible active sites in the selective aerobic oxidation of *n*-butane to MA [6,11,12]. These active species could be independent of the crystalline structure of VPO catalysts since the completely amorphous VPO catalysts can eliminate the long induction period with higher intrinsic activity [13]. Wachs et al. investigated VO_x catalysts supported on various metal oxides and all tested catalysts produced MA via the *n*-butane oxidation [14]. Introducing phosphate to the supported VO_x catalysts increased MA selectivity from 23% to 56%, but the VPO structure and δ-$VOPO_4$-like phases were absent as evidenced by *in situ* Raman spectroscopy [14]. These

* Corresponding authors.
E-mail addresses: michael.hunger@itc.uni-stuttgart.de (M. Hunger), alfons.baiker@chem.ethz.ch (A. Baiker), jun.huang@sydney.edu.au (J. Huang).

https://doi.org/10.1016/j.jcat.2022.06.013
0021-9517/© 2022 Published by Elsevier Inc.



Scheme 1. Aerobic oxidation of *n*-butane to form maleic anhydride.

studies demonstrate that the supported VO_x catalysts are catalytically active sites, which could work in conjunction with phosphate to promote the reaction.

Exploring surface-active VO_x species on the supported VO_x catalysts is attractive to improve their activity in the selective aerobic oxidation of *n*-butane to MA, alternatively to VPO catalysts. However, the identification and control of surface sites on the supported VO_x catalysts is quite challenging due to the existence of various V structures (single sites, clusters, nanoparticles, and crystals) and surface functional groups (V = O, V-O-V, and V-OH). Mainly single-site VO_x (SSV) is generated on a silica support, affording a MA selectivity of 91.8% [15,16], but the activity of SSV is questioned by the extremely low *n*-butane conversion (2.8%). On alumina-supported VO_x catalysts, 2.5 times higher *n*-butane conversion was achieved in the presence of both SSV and cluster VO_x under the same conditions [16,17]. At high V loading or on vanadium oxide, lattice oxygen has been proposed to be involved in the catalytic oxidation of hydrocarbons through a Mars-Van Krevelen mechanism [18] where the oxygen vacancy generated can capture an O_2 molecule to rearrange the structure. These comparative studies were based on VO_x supported on different carriers with various structures and functional groups on the surface. Therefore, the determination of active sites in supported VO_x catalysts for efficient oxidation of n-butane to MA is still a matter of debate.

Flame-spray pyrolysis (FSP) is a simple, rapid, and scalable technique for the synthesis of multi-composition nanoparticles [19–21]. FSP can provide homogeneous dispersion/mixing of multi-components, which is often difficult to achieve with other classical preparation techniques [22]. As an example, single-site Al is generated in flame-made amorphous silica-alumina (Al/Si = 1/9) [23,24]. Under the same synthesis conditions, two or more Al sites in proximity are probed in the flame-made amorphous silica-alumina (Al/Si $\geq$ 5/5) with increasing the surface Al density [24]. Since the V structures depend on the surface V density (**Fig. S1**) [25–28], the synthesis of V/Al_2O_3 catalysts using FSP is expected to promote the formation of VO_x species from SSV to nanocrystals by simply increasing the V/Al ratio under the same conditions.

In this work, we synthesized V/Al_2O_3 catalysts of various V/Al ratios by the FSP method for the selective oxidation of *n*-butane to MA, aiming at shedding new light on possible active sites and the governing reaction mechanism. VO_x structures from SSV to nanocrystals are characterized using XRD, UV–vis, Raman, and solid-state NMR spectroscopy, as well as in characterizing penta-coordinated Al (Al^V) species as defect sites and crystalline $AlVO_4$. The combination of different VO_x structures and surface defects provides a chance to identify the catalytic active sites and their possible cooperativity with surface functional groups in the *n*-butane oxidation to MA. The structure–reactivity relationship will be discussed and a reaction mechanism based on SSV-Al^V pairs is proposed.

2. Experimental

2.1. Catalyst preparation

V/Al_2O_3 nanoparticles were synthesized using the FSP method as described elsewhere [19]. Firstly, a solution of 2-ethylhexanoic acid (2-EHA, Riedel-de Haën, >99%) and acetic anhydride (Riedel-de Haën, >99%) in a ratio of 2:1 (vol%) was prepared. Then, the appropriate amount of ammonium metavanadate (Sigma–Aldrich, 99%) was added to the above solution under stirring and heating at 373 K for several hours, resulting in a metal concentration of 0.5 M. Next, the desired amounts of aluminum(III) acetylacetonate (99%, ABCR) and the vanadium precursor were mixed with the desired nominal mole ratio of V/Al in the catalysts with xylene (Riedel-de Haën, >96%) and 2-EHA (Riedel-de Haën, >99%) in a ratio of 1:1 (vol%). The use of solvents (xylene, 2-EHA) can provide a high combustion enthalpy to assist particle formation in FSP [29,30]. The resulting solution was filtered using a glass filter, pumped through a capillary at a rate of 5 mL/min, and nebulized with 5 L/min O_2 for high dispersion of the liquid precursor spray. The resulting spray was ignited by an annular supporting methane/oxygen flame (1.5/3.3 L/min). The powders were collected on a cooled Whatman GF6 filter (257 mm diameter) with the aid of a vacuum pump (Busch SV 1040C). All produced samples were dissolved in HF solution and analyzed by atomic emission spectroscopy with an inductively coupled plasma (ICP-AES, Perkin–Elmer, Plasma 400). The nomenclature of V/Al_2O_3 catalysts and the results of the chemical analysis are listed in Table 1.

2.2. Catalyst characterization

X-ray diffraction (XRD) patterns of V/Al_2O_3 samples in the range of 10-70° were recorded on a Siemens D6000e diffractometer using Cu-Kα radiation (λ = 0.154 nm, 35 kV, 40 mA) and scanning steps of 0.02°.

N_2 adsorption/desorption isotherms of V/Al_2O_3 samples were measured on an Autosorb IQ-C system and the specific surface areas of the samples were determined using the Brunauer–Emmett–Teller (BET) method. Before the adsorption measurements, about 50 mg of each sample was degassed at 423 K for 12 h under vacuum. Measurements were carried out at 77 K.

Diffuse reflectance-UV–vis spectra were recorded in the range of 200–800 nm on a Cary 5 instrument equipped with a 'Praying Mantis' attachment from Harrick.

Raman spectroscopy was performed (Renishaw InVia Reflex Raman) with a 514-nm diode (Ar-ion laser, 25 mW) laser as an excitation source focused with a microscope (Leica, magnification 50). The spectra were recorded after 20 accumulations to warrant an adequate signal-to-noise ratio and collected on a CCD camera after being diffracted by a prism (1800 lines per millimeter) using 12.5-mW laser energy.

Solid-state MAS NMR experiments were performed at room temperature on a Bruker AVANCE III 400WB spectrometer using a 4-mm MAS NMR probe. The ^{51}V and ^{27}Al spectra were recorded at a spinning rate of ca. 12 or 14 kHz with a resonance frequency of 105.25 MHz and 104.26 MHz, respectively. NMR measurements were done on as-prepared (hydrated) and dehydrated samples. In

Table 1
Compositions, specific surface areas (SSA), and V surface densities of flame-made V/Al_2O_3 catalysts.

Sample [a]	V content (atom%)	V content [b] (atom%)	SSA [c] m^2/g	V-density (#V/nm^2)
SSV	10	12	132	8
PV-1	20	21	93	22
PV-2	30	29	68	42
CV-1	70	72	103	52
CV-2	100	100	50	134

[a] SSV, PV, and CV represent single-site V, polymeric V, and crystalline VO_x, respectively. [b] V content from ICP analysis. [c] SSA from BET analysis of N_2 adsorption/desorption isotherms. [d] The V densities are estimated based on the VO_x content and SSA.

the latter case, the catalysts were dehydrated in a furnace at 773 K with a ramp of 10 K/min for 2 h under vacuum. Subsequently, the dehydrated catalyst was transferred without any contact to air into a glove box purged with dry N_2 and filled into the 4-mm MAS rotor. In the experiments, a single pulse length of $\pi/8$ and $\pi/6$ with a relaxation delay of 0.5 s and 1 s were used for ^{51}V and ^{27}Al MAS NMR measurements, respectively. The ^{51}V chemical shift was referenced to vanadium trichloride oxide ($VOCl_3$). The NMR data were processed with the Bruker software WINNMR. Anisotropic shift values were obtained from the simulated MAS NMR spectra with the Bruker WINFIT software.

2.3. Catalytic reaction

The selective oxidation of *n*-butane on the different catalysts was investigated using a fixed-bed laboratory reactor with an inner diameter of 8 mm. Before the catalytic tests, the catalyst was pressed, crushed, and fractioned (200–315 μm). Then 200 mg catalyst was diluted with 2 g SiC (500–630 μm) resulting in a catalytic bed length of ca. 10 mm. The catalysts were activated at 773 K in synthetic air (100 mL/min) for 1 h and then cooled down to the reaction temperature. The catalytic reaction was performed under a flow of *n*-butane (0.3 mL/min) and synthetic air (4.5, 9.7, 19.7 mL/min) at atmospheric pressure and temperatures in the range of 593–738 K. The flow rate of each gas was controlled by specific mass flow controllers. The gas mixture was balanced by dry N_2 with a total gas flow rate of 20 mL/min. The time interval for data collection was ca. 15 min. The reaction products were analyzed by an online gas chromatograph HP 6890 equipped with a HP-5 column (30 m × 0.32 mm × 0.5 μm).

The stability of the V/Al_2O_3 catalysts was tested under optimized conditions. The spent catalyst was regenerated through *in situ* calcination in air at 773 K for 1 h and then cooled down to the reaction temperature.

3. Results and discussion

3.1. Material characterization

The compositions and specific surface areas of the flame-made V/Al_2O_3 catalysts are summarized in Table 1. The V content determined by ICP analysis confirms the compositions of V/Al_2O_3 catalysts as preselected by the amounts of the precursors. The SSV catalyst exhibited the highest surface area of 132 m^2/g, which decreased to 68 m^2/g when increasing the V/Al ratio to 3/7 in PV catalysts. This is similar to those observed with V/Al_2O_3 catalysts when increasing the V content from 5 to 30 wt% [31–33]. Thereafter, the surface area of the CV-1 catalyst significantly increased to 103 m^2/g, which is much higher than that of vanadium oxide (CV-2) 50 m^2/g. The high surface area of the CV-1 catalyst indicates compositional/structural changes compared to the other V/Al_2O_3 catalysts. Often, the formation of different VO_x structures, such as single-site V (SSV), polymeric V (PV), and crystalline VO_x (CV) schematically shown in **Fig. S1**, on the support depends on the surface V density, for instance, SSV at < 2.3 V/nm^2, PV at 2.3–7.5 V/nm^2, and CV at > 8 V/nm^2 [25–28]. Therefore, a significant compositional/structural change of V species on V/Al_2O_3 catalysts is expected with the rapid increase of the surface V density from 8 to 134 V/nm^2 here.

The compositional/structural changes of V/Al_2O_3 catalysts were confirmed by their XRD patterns. Fig. 1**a** shows the typical XRD pattern of V_2O_5 (JCPDS card No. 41–1426) for the CV-2 catalyst [34,35]. The diffraction peaks became broad and their intensity decreased with increasing Al content. In addition to V_2O_5, the reflections of $AlVO_4$ (JCPDS card No. 39–276) were detected in

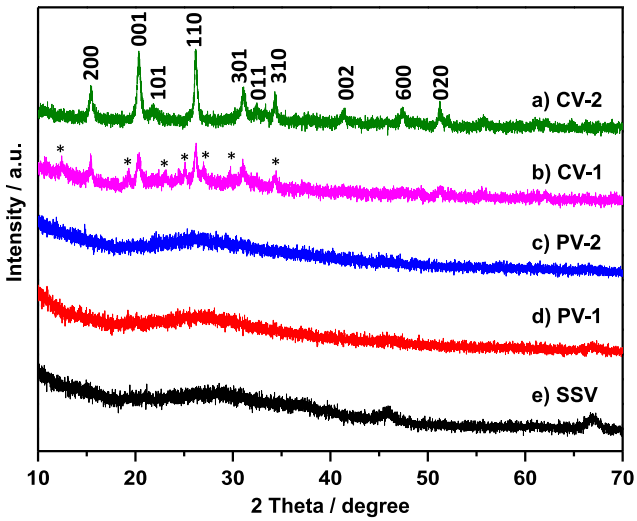


Fig. 1. XRD pattern of the V/Al_2O_3 catalysts (a) CV-2, (b) CV-1, (c) PV-2, (d) PV-1, and (e) SSV. The 2 Theta reflections indicative of $AlVO_4$ are marked by * in the pattern.

the pattern of the CV-1 catalyst (Fig. 1**b**). The reflections of crystalline V_2O_5 and $AlVO_4$ were both absent in SSV and PV catalysts (Fig. 1**c-e**). For SSV and PV-1 catalysts, the observed weak and broad peaks at ca. 46° and 77° were attributed to amorphous alumina (JCPDS card No. 10–0425). The absence of V_2O_5 reflections in the XRD patterns (Fig. 1**c-e**) indicates that the V species are present in very small particles or clusters [36], which are not discernible by XRD. Note that this contrasts with the previous observations at such high V surface density (>8.3 V/nm^2), which mainly showed crystalline V_2O_5 species as observed in sol–gel prepared V/Al_2O_3 catalysts [25–28].

TEM images and EDX mapping were applied to investigate the controversy between the XRD pattern and the surface V density of V/Al_2O_3 catalysts. Compared to the conventional wet-chemistry techniques, FSP synthesis is widely reported to promote the formation of homogeneously mixed metal oxides [37–39]. Homogeneous distribution of vanadium on the alumina surface at low V content is shown for the SSV catalyst in Fig. 2**a-c**. Small particles with alumina lattice structure could be identified in Fig. 2**d** and confirmed by the corresponding fast-Fourier transform (FFT) pattern, in line with the diffraction peaks observed in Fig. 1**e**. No clear lattice structure of VO_x can be detected in Fig. 2**d** confirming the high dispersion of VO_x, in line with the absence of V_2O_5 peaks in its XRD pattern. By increasing the V content (e.g. PV-2), the aggregation of some VO_x species results in small VO_x nanoparticles with lattice structure (e.g. for V_2O_5) as shown in Fig. 2**e-h**. In addition, part of the V species are incorporated into the alumina matrix, forming $AlVO_4$ (Fig. 2**h**). The particle sizes of V_2O_5 and $AlVO_4$ on the PV-2 catalyst are in the range of 2–5 nm and thus hardly detectable by XRD, as shown in Fig. 1**c**. At high V content, the EDX mapping analysis shows that the CV-1 catalyst mainly consisted of V_2O_5 but a significant fraction of V_2O_5 particles could be observed in the TEM image along with $AlVO_4$ particles (Fig. 2**i-l**), which correlates well with the peaks of V_2O_5 and $AlVO_4$ observed in corresponding XRD pattern (Fig. 1**i**). The lack of a V_2O_5 phase or nanoparticles in SSV and PV catalysts demonstrates that using FSP significant aggregation or sintering of VO_x species, which occurs during the high-temperature calcination used in other synthesis methods, can be avoided. Therefore, FSP can promote the homogeneous distribution and population of VO_x species on the alumina surface at relatively high surface V densities (e.g. 8.3 V/nm^2 for SSV catalyst), whereas at similar surface V densities,

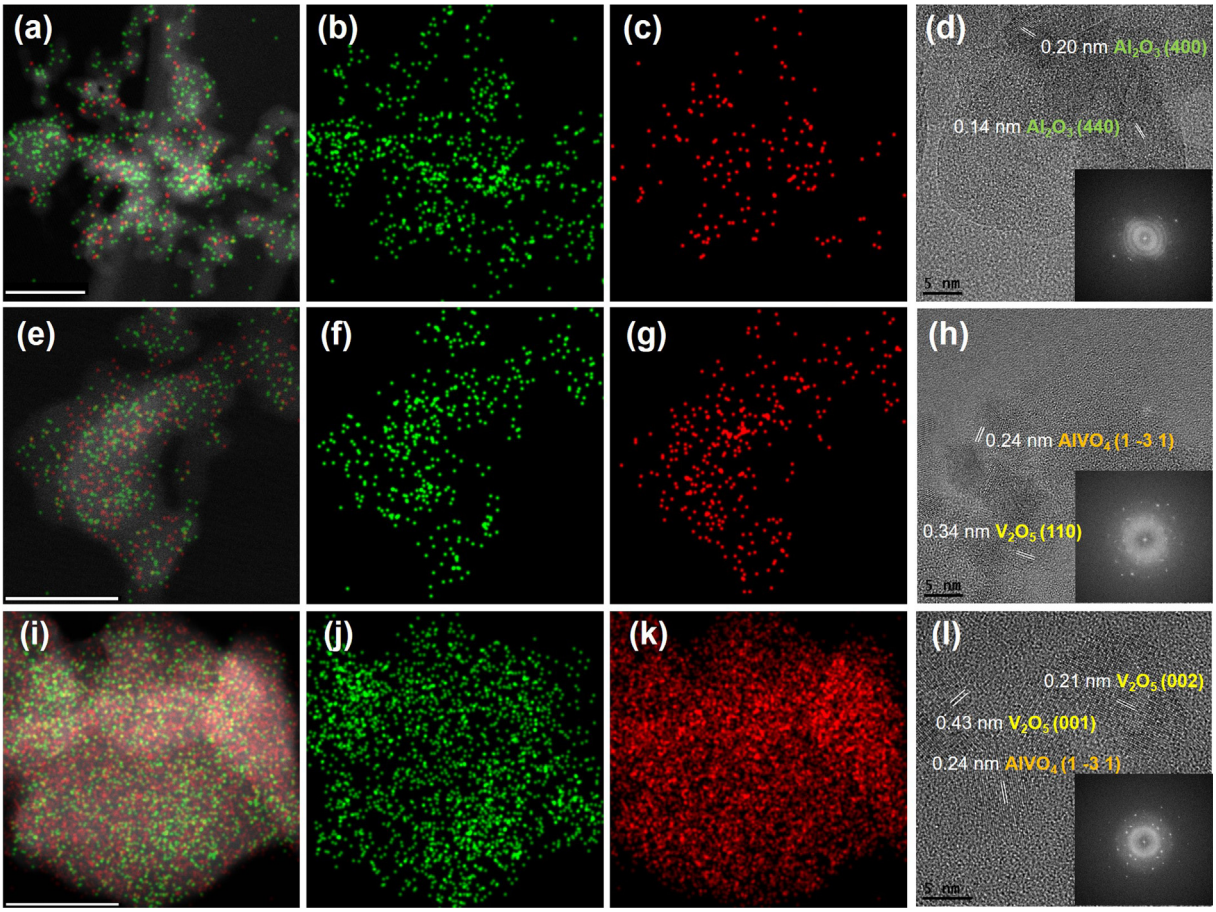


Fig. 2. EDX and TEM images of the V/Al_2O_3 catalysts (a-d) SSV, (e-h) PV-2, and (i-l) CV-1. Green spots for Al and red spots for V.

mainly bulk-like V_2O_5 (>8 V/nm^2) were observed for previous supported VO_x catalysts. If the VO_x species are active sites as proposed, the high population of VO_x species in V/Al_2O_3 catalysts is expected to promote the selective oxidation of *n*-butane.

UV–vis spectroscopy was applied to scrutinize the VO_x species formed on the V/Al_2O_3 catalysts. UV–vis can probe different electronic transitions for isolated and polymeric VO_x structures, and the edge energy (E_g) obtained correlates to the dispersion of surface VO_x. The UV–vis spectra, together with the band positions and the edge energies are displayed in Fig. 3. SSV and PV catalysts showed the main absorption band in the region of 227–290 nm, which corresponds to SSV species [40,41]. A redshift was observed with increasing V content, hinting at a higher coordination number of vanadia species [42,43]. For comparison, the spectrum of the CV-2 catalyst is typical for vanadium oxides reported in the literature [44]. Additional shoulders at 348 nm and 413–478 nm are attributed to the presence of polymeric tetrahedral V^{5+} species and "bulk-type" polymeric V_2O_5-like vanadium species on CV catalysts [40,41]. Compared to polymeric VO_x, isolated VO_x has a lower electron delocalization, and thus, is often characterized by a higher E_g. Similar trends were observed with V/Al_2O_3 catalysts. Increasing the dispersion of V on the alumina support by decreasing the V content from 100% to 10% results in a significant increase of the corresponding E_g from 1.12 eV to 1.94 eV. The obtained E_g of isolated VO_x is a bit lower than those obtained with isolated VO_x on SiO_2 [45], which could be influenced by several parameters, such as the local structure, the polarization effect and the support properties [46,47]. No adsorption bands for electron *d-d* transitions in the 600–800 nm region could be detected in all samples [48], indicating that the formation of V^{4+} ions in the current V/Al_2O_3 catalysts is unfavorable.

Raman spectroscopy was employed to study the vibrations of surface VO_x species. Fig. 4**a** shows a sharp Raman band at 995 cm^{-1} for the vanadyl V = O bond associated with multiple sharp bands at lower wavenumbers for bridging V-O-V bonds, typical for bands of crystalline V_2O_5 species [49]. The Al_2O_3 support allows direct access to vanadium oxide vibrations in the V/Al_2O_3 catalysts by Raman spectroscopy [50]. The CV-1 catalyst (Fig. 4**b**) shows similar bands to vanadium oxide (CV-2), hinting at crystalline V_2O_5 nanoparticles and/or a bulk V_2O_5 phase are dominant,

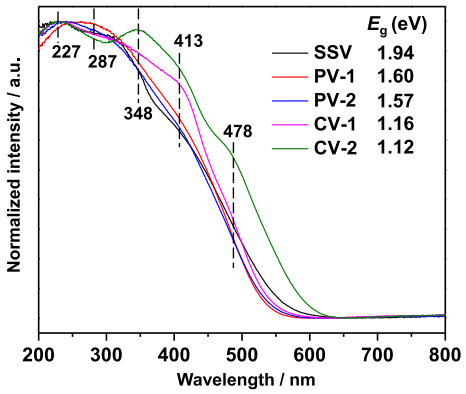


Fig. 3. UV–vis spectra of V/Al_2O_3 catalysts.

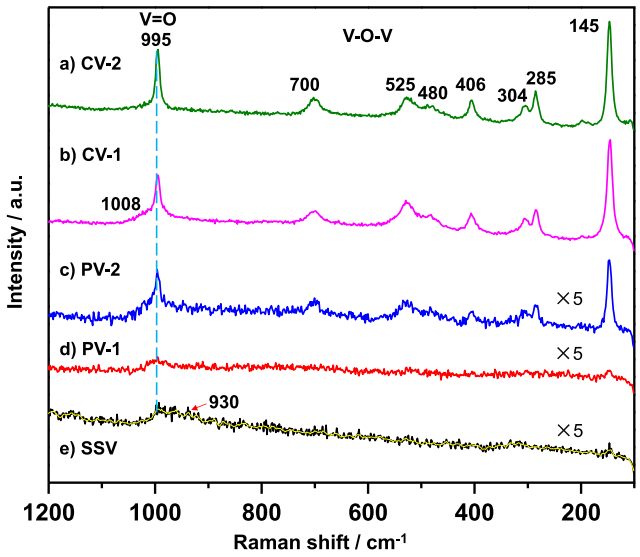


Fig. 4. Raman spectra of the V/Al_2O_3 catalysts (a) CV-2, (b) CV-1, (c) PV-2, (d) PV-1, and (e) SSV.

in line with the corresponding XRD pattern. These Raman bands became broader when reducing the V content from 100% to 30% (Fig. 4**c**), demonstrating a loss of long-range order of the supported VO_x species with decreasing V surface density. The Raman bands of V_2O_5 species almost disappeared for PV-1 and SSV catalysts (Fig. 4**d and 4e**), indicating very low polymerization of VO_x species, which confirms a high dispersion of VO_x species on the alumina surface, as observed above. Besides the above bands, a broad band at ~1008 cm^{-1} for terminal V = O vibration of the surface VO_4 species [51–53] is observed with the CV-2 catalyst and arises with decreasing V content to 30% (PV-2). The significant increase in the relative intensity of terminal V = O at lower V content is promoted by improving the distribution of VO_x species on the alumina surface. However, the band at ~1008 cm^{-1} for the terminal V = O and the band at 995 cm^{-1} for the vanadyl V = O bond are hardly to be observed in Fig. 4**d and 4e**. The absence of these V = O species demonstrates that the V species are well dispersed on alumina supported in the SSV and PV-1 catalysts, which could form the bridging V–O–Al as indicated by a weak band at 930 cm^{-1} in the PV-1 and SSV catalysts [54].

All V surface species identified by the above-mentioned investigations have the oxidation state 5 + and are diamagnetic. To gain deeper insights, the local structure of V/Al_2O_3 catalysts was characterized by solid-state NMR spectroscopy.

The ^{51}V MAS NMR spectra of hydratedV/Al_2O_3 catalysts are shown in **Fig. S2**. To elucidate sideband patterns for assigning the central line, ^{51}V MAS NMR spectra of all samples were recorded with spinning rates of 12 and 14 kHz, since the chemical shift of the central line remained unchanged at different spinning rates while the peaks of sidebands patterns shifted dependently. The main peak at δ_{51V} = -617 ppm and three weak peaks at δ_{51V} = -671, −690, −735, and −785 ppm can be well distinguished for the CV-1 catalyst, while the peaks at δ_{51V} = -430 ± 5 ppm, and −510 ± 5 ppm are dominant in PV and SSV catalysts.

The chemical shift parameters of the hydrated catalysts summarized in Table 2 are derived from simulating the ^{51}V MAS NMR spectra at 14 kHz as shown in Fig. 5. For the CV-1 catalyst, the peak at δ_{51V} = -617 ppm is typically observed in bulk-like V_2O_5 [55,56]. The obtained isotropic chemical shifts at δ_{51V} = -671, −735, and −785 ppm, as well as corresponding anisotropic chemical shift parameters, are similar to those reported in the literature for $AlVO_4$.(δ_{51V} = -668 ± 5 ppm, −747 ± 5 ppm, and −780 ± 5 ppm), which consists of three symmetry-inequivalence of VO_4^{3-} tetrahedral [56–58]. The peak at δ_{51V} = -690 ppm is mainly observed with the CV-1 catalyst and is assigned to polymeric tetrahedral VO_4 species. However, these peaks in the spectra of CV-1 are hardly discernible with PV and SSV catalysts, which indicates that both crystalline V_2O_5 and $AlVO_4$ are less favored at low V content, well in line with the XRD analyses. No obvious peak features of tetrahedral VO_4 species in the range of −600 to −800 ppm could be detected in the hydrated PV-1 and SSV catalysts, which may hint at the high dispersion, accessibility, and reactivity of the surface V sites (Figs. 1-4), in contrast to sol–gel derived materials with similar V loading [55,56,59–61]. Instead, a main peak at δ_{51V} = -510 ± 5 ppm and a weak peak at δ_{51V} = -430 ± 5 ppm are detected in PV-1 and SSV catalysts. These peaks are assigned to the decavanadate polyanions ($V_{10}O_{28}^{6-}$) that are usually present under hydrated conditions [55,62].

Dehydrated V/Al_2O_3 catalysts were investigated using ^{51}V MAS NMR spectroscopy to elucidate the possible active sites since they extensively work under dehydration conditions. Upon dehydration, the transformation of VO_x species (e.g. octahedral vanadia species at δ_{51V} = -340 to −360 ppm) [57,59] into tetrahedral VO_4 species on the alumina support has been widely reported, while very limited change could be observed in the original tetrahedral VO_4 species (δ_{51V} = -600 to −800 ppm, most could be in the non-surface region) [57]. Similar behavior was also observed here, and thus, mainly the ^{51}V MAS NMR spectra of PV and SSV catalysts with significant changes after dehydration are shown. Again, the spectra of all samples were recorded with spinning rates of 12 and 14 kHz to assign the central lines (**Fig. S3**). Strong peaks at δ_{51V} = -690, −727 ± 5, 740 ± 5, and −785 ± 5 ppm, and a weak peak

Table 2
Chemical shift parameters of the hydrated V/Al_2O_3 catalysts.

Hydrated catalyst	Isotropic chemical shift δ_{iso} (ppm)	Anisotropic chemical shift tensor (ppm)			Concentration (%)
		δ_{11}	δ_{22}	δ_{33}	
CV-1	−617 (V-O-V)	93	−449	−1495	88.4
	−671 ($AlVO_4$)	−18	−520	−1474	2.2
	−690 (polymeric VO_4)	−681	−686	−702	1.3
	−737 ($AlVO_4$)	−486	−842	−853	6.7
	−785 ($AlVO_4$)	369	−852	−1862	1.4
PV-2	−430 ($V_{10}O_{28}^{6-}$)	−145	−259	−886	14.2
	−510 ($V_{10}O_{28}^{6-}$)	−151	−419	−960	68.9
	−617 (V-O-V)	−158	−218	−1475	16.9
PV-1	−430 ($V_{10}O_{28}^{6-}$)	−155	−467	−668	2.9
	−510 ($V_{10}O_{28}^{6-}$)	−75	−448	−1007	97.1
SSV	−431 ($V_{10}O_{28}^{6-}$)	−26	−486	−781	5.2
	−508 ($V_{10}O_{28}^{6-}$)	−102	−528	−894	94.8

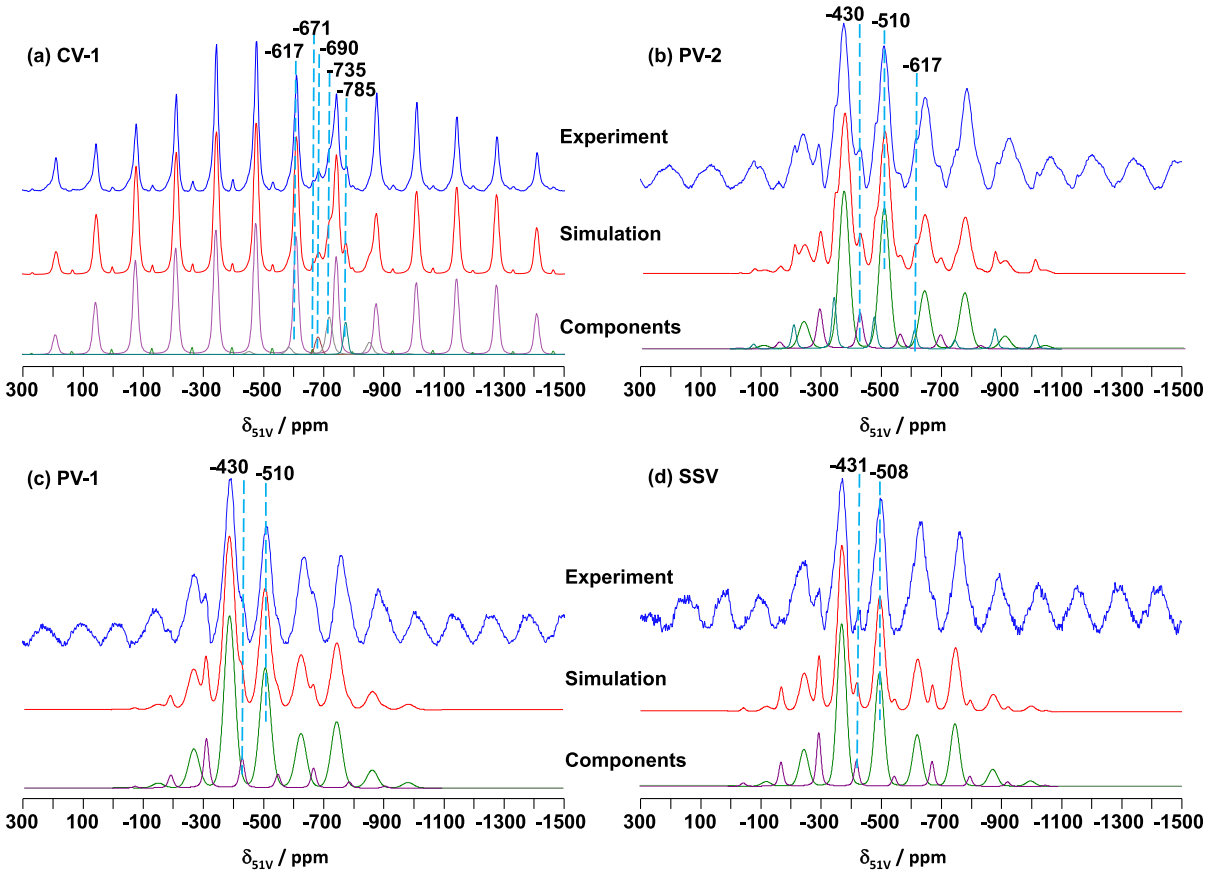


Fig. 5. ^{51}V MAS NMR spectra of the hydrated V/Al_2O_3 catalysts (a) CV-1, (b) PV-2, (c) PV-1, (d) SSV. Experiment (top), simulation line (middle), and components (bottom).

Table 3
Chemical shift parameters of the dehydrated V/Al_2O_3 catalysts.

Dehydrated sample	Isotropic chemical shift δ^a_{iso} (ppm)	Anisotropic chemical shift tensor[b] (ppm)			Concentration (%)
		δ_{11}	δ_{22}	δ_{33}	
PV-2	−644 ($AlVO_4$)	−593	−601	−798	0.5
	−690 (polymeric VO_4)	−601	−606	−863	10.2
	−727 (polymeric VO_4)	−610	−619	−952	22.9
	−740 ($AlVO_4$)	−662	−670	−888	36.1
	−785 ($AlVO_4$)	−679	−686	−990	30.3
PV-1	−644 ($AlVO_4$)	−556	−580	−857	13.7
	−690 (polymeric VO_4)	−557	−580	−932	1.9
	−723 (polymeric VO_4)	−575	−600	−993	5.0
	−747 ($AlVO_4$)	−613	−648	−977	30.4
	−780 ($AlVO_4$)	−630	−659	−1051	49.0
SSV	−664 (Al-O-V)	−481	−522	−989	58.9
	−764 (Al-O-V)	−591	−841	−860	41.1

at δ_{51V} = -664 ppm are observed in PV catalysts, while only two peaks at δ_{51V} = -664 and −740 ± 5 ppm are dominant in the SSV catalyst.

The chemical shift parameters of the dehydrated catalysts summarized in Table 3 are derived from simulating the ^{51}V MAS NMR spectra at 14 kHz as shown in Fig. 6. In all cases, the peaks at δ_{51V} = -430 ± 5 and −510 ± 5 ppm observed for decavanadate at hydrated conditions disappeared. Meanwhile, the peaks (δ_{51V} = -664∼-666 ppm, −740∼-746 ppm, and −780∼-786 ppm) at the similar chemical shifts of $AlVO_4$ species increased dramatically in PV catalysts. Decavanadate can be decomposed into monomeric $[VO_4]^{3-}$, dimeric $[V_2O_7]^{4-}$ or tetrameric $[V_4O_{12}]^{4-}$, which is usually carried out at 403 K < *T* < 693 K or at ambient temperature and pH > 7 [63,64]. The rearrangement of the local structure with these small oxovanadates at the alumina surface can result in vanadates, such as $AlVO_4$ clusters, in line with the observation in Fig. 2**h**. Therefore, the sharp peaks at δ_{51V} = -664∼-666 ppm, −740∼-746 ppm, and −780∼-786 ppm, in PV catalysts are attributed to the three inequivalent tetrahedral VO_4 in $AlVO_4$. Thus the peaks at δ_{51V} = -690 and −727 ± 5 ppm are assigned to the tetrahedral VO_4 species in polymeric vanadates originating from decavanadate decomposition since the polymeric vanadates from vanadia in CV catalysts are hardly discernible in the ^{51}V spectra of PV catalysts under hydrated conditions (Fig. 5 **and S2**). This is confirmed further by the absence of the peaks at δ_{51V} = -690 and −727 ± 5 ppm in the SSV catalyst that can provide a high

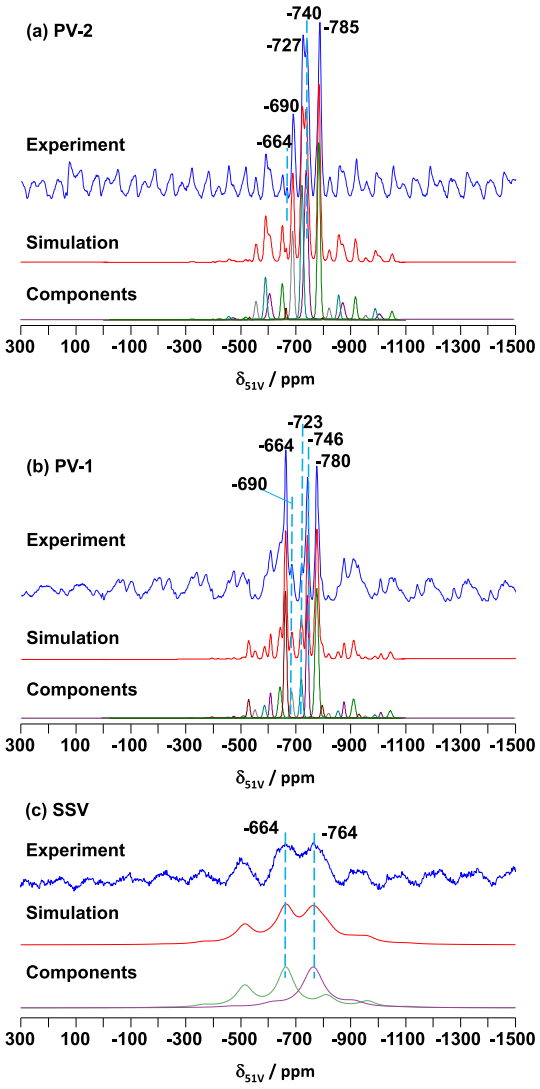


Fig. 6. ^{51}V MAS NMR spectra of the dehydrated (773 K) V/Al_2O_3 catalysts (a) PV-2, (b) PV-1, and (c) SSV. Experiment (top), simulation line (middle) and components (bottom).

dispersion of V species. Instead, very broad peaks centered at δ_{51V} = -664 and −764 ppm are detected in SSV catalysts (Fig. 6**c**), replacing the three sharp peaks typically observed for $AlVO_4$ clusters as observed in Fig. 6**a and 6b**. The missing of inequivalent tetrahedral VO_4 in $AlVO_4$ suggests that the VO_4 species from decavanadate decomposition can be coordinated to surface Al defects, forming Al-O-V linkages similar to those observed in the $AlVO_4$ structure, which correlates well with no $AlVO_4$ clusters observed in Fig. 2**d**. Compared to the SSV catalyst, the formation of $AlVO_4$ clusters in the PV catalysts could be caused by the much lower surface areas and the significantly higher contents of decavanadate at high V contents. The broad line shape indicates that these V species in the SSV catalyst show a wide distribution with various surface defects. This could be supported by comparing the anisotropic chemical shift tensors (Table 3), which demonstrates that the Al-O-V linkages in the SSV catalyst are strongly distorted compared to those in the PV catalysts. The $AlVO_4$–like Al-O-V linkages could be also generated in the PV catalysts in addition to the $AlVO_4$ clusters.

The local structure of V/Al_2O_3 catalysts was further confirmed by ^{27}Al MAS NMR spectroscopy (Fig. 7). In addition to the three inequivalence of VO_4^{3-} tetrahedra observed in the ^{51}V MAS NMR

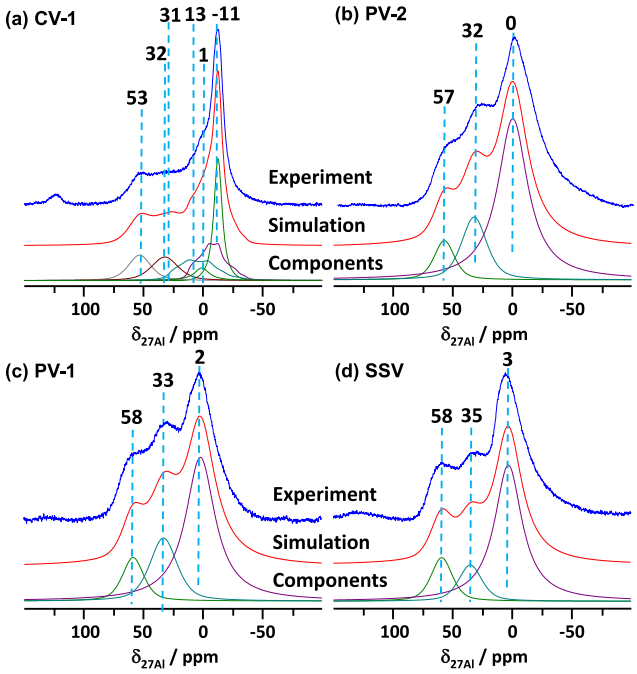


Fig. 7. ^{27}Al MAS NMR spectra of the hydrated V/Al_2O_3 catalysts (a) CV-1, (b) PV-2, (c) PV-1 and (d) SSV. Experiment (top), simulation line (middle) and components (bottom).

spectra, the structure of $AlVO_4$ consists of two AlO_6 octahedra (at δ_{27Al} = 15∼-30 ppm), and a penta-coordinated AlO_5 unit (at δ_{27Al} = 40∼25 ppm), which has been confirmed by the ^{27}Al 3QMAS NMR spectrum of $AlVO_4$ [58]. The ^{27}Al MAS NMR spectrum of hydrated CV-1 catalyst consists of a strong Al^{VI} peak at δ_{27Al} = -11 ppm with a broad hump at high frequency, as well as Al^{V} and Al^{IV} peaks centered at δ_{27Al} = 31 ppm and 53 ppm, respectively. By simulating the spectrum, two Al^{VI} species (at δ_{27Al} = -11 ppm and 13 ppm) and one Al^{V} species (at δ_{27Al} = 31 ppm) have been identified for $AlVO_4$, well in agreement with the chemical shift parameters and line shape reported in the literature [58,65]. Three peaks at δ_{27Al} = 53, 32, and 1 ppm are involved in weak quadrupolar interaction under hydration conditions (Table 4), which are assigned to Al^{IV}, Al^{V} and Al^{VI} species in small alumina

Table 4
Chemical shift parameters of the dehydrated V/Al_2O_3 catalysts.

Hydrated sample	Chemical shift δ_{iso}[a] (ppm)	C_{QCC} MHz	η	Concentration (%)
CV-1	−11 ($AlVO_4$)	1.7	0.35	25.5
	13 ($AlVO_4$)	5.8	0.65	22.0
	31 ($AlVO_4$)	6.8	0.45	17.7
	53 (Al^{IV})		0.5	14.0
	32 (Al^{V})		0.5	15.2
	1 (Al^{VI})		0.5	5.6
PV-2	57 (Al^{IV})		0.5	9.6
	32 (Al^{V})		0.5	19.1
	0 (Al^{VI})		0.5	71.3
PV-1	58 (Al^{IV})		0.5	11.8
	33 (Al^{V})		0.5	21.9
	2 (Al^{VI})		0.5	66.3
SSV	58 (Al^{IV})		0.5	15.0
	35 (Al^{V})		0.5	13.7
	3 (Al^{VI})		0.5	71.3

[a] Isotropic chemical shifts (δ_{iso}), quadrupole coupling constant (C_{QCC}), and asymmetry parameters of the electric field gradient tensor (η) of each aluminum species, determined by simulation of ^{27}Al MAS NMR spectra of hydrated V/Al_2O_3 catalysts.

clusters/particles or a mixed-phase between vanadia and alumina since no alumina phase could be observed in the XRD pattern of the CV-1 catalyst. The peaks assigned to the $AlVO_4$, particularly δ_{27Al} = -11 ppm, are disappeared in the ^{27}Al MAS NMR spectra of PV and SSV catalysts, in line with the absence of $AlVO_4$ in their ^{51}V MAS NMR spectra (Fig. 5). Mainly Al^{IV}, Al^{V} and Al^{VI} species in small alumina clusters/particles or mixed-phase between vanadia and alumina could be observed with the PV and SSV catalysts since they are XRD amorphous. Previous reports show that the formation of Al^{V} species at high Al content is attributed to the heteroatoms (e.g. Si), which are incorporated and disturb the local structure of the alumina matrix, while hydrated FSP-derived alumina displays no Al^{V} species [22,30,39]. Since mainly the decavanadate polyanions ($V_{10}O_{28}^{6-}$) could be observed in the ^{51}V spectra of PV and SSV catalysts, connectivity between decavanadate polyanions and Al^{V} species is supposed. This connectivity provides a high possibility for the VO_4 species stemming from decavanadate decomposition to interact with surface Al defects (e.g. Al^{V}), forming Al-O-V linkages as observed in Fig. 6.

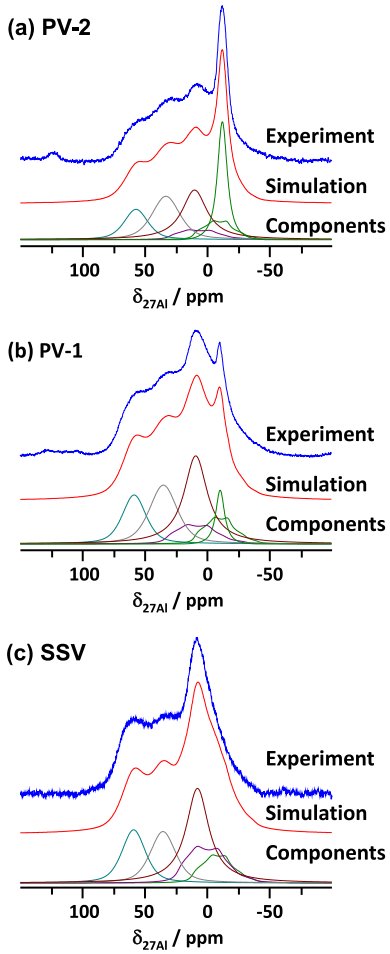


Fig. 8. ^{27}Al MAS NMR spectra of the dehydrated (773 K) V/Al_2O_3 catalysts (a) PV-2, (b) PV-1 and (c) SSV. Experiment (top), simulation line (middle), and components (bottom).

Upon dehydration of the V/Al_2O_3 catalysts, the peak at δ_{27Al} = ~-11 ppm was clearly observed with the PV catalysts in Fig. 8**a and 8b**. The sharp peak at δ_{27Al} = -11 ppm demonstrates that the $AlVO_4$ species absent in the hydrated state could be generated after dehydration, which correlates well with those observed from ^{51}V MAS NMR spectra. However, Fig. 8**c** shows the absence of the peak at δ_{27Al} = -11 ppm in the SSV catalyst, which confirms the formations of mainly highly dispersed tetrahedral VO_4 species, other than $AlVO_4$ clusters. Overlapping the ^{27}Al MAS NMR spectra of V/Al_2O_3 catalysts before and after dehydration (**Fig. S4**) demonstrates that the $AlVO_4$ species are generated from Al^{V} and Al^{VI} species in the PV and SSV catalysts upon dehydration. Based on these observations the ^{27}Al MAS NMR spectra were simulated, as shown in Fig. 8. As observed in crystalline $AlVO_4$ and those in Fig. 6, two AlO_6 octahedra (at δ_{27Al} = 15 ~ -11 ppm), and a penta-coordinated AlO_5 unit (at δ_{27Al} = 40 ~ 31 ppm) are characterized in the PV catalysts. In the SSV catalyst, AlO_6 octahedra (at δ_{27Al} = -11 ppm) are absent, in line with the absence of an inequivalent tetrahedral VO_4 of $AlVO_4$ as shown in Fig. 6. The SSV catalyst shows a similar content of AlO_6 octahedra (at δ_{27Al} = 13 ppm), but the penta-coordinated AlO_5 unit (at δ_{27Al} = 40 ~ 31 ppm) is ~2-3 times that of the PV catalysts.

The supported vanadia on dehydrated metal oxides (e.g. Al_2O_3) can be solvated and polymerized upon rehydration [7,66]. The coordination of solvated vanadia depends on both the concentration of vanadium and the overall pH of the material and is independent of the vanadium precursor or preparation techniques [66,67]. Increasing surface V concentration promotes the polymerization of SSV species to vanadium oxide (**Fig. S1**). The recovery of decavanadate at a V surface density of 4 V/nm^2 upon rehydration of dehydrated V/Al_2O_3 catalysts has been reported earlier [55]. Therefore, at a V surface density > 8 V/nm^2, the formation of decavanadate in rehydrated V/Al_2O_3 was examined. As an example, the ^{51}V and ^{27}Al MAS NMR spectra of the dehydrated PV-1 catalyst recorded before and after rehydration are shown in **Fig. S5**. Almost the same line shapes in the ^{51}V and ^{27}Al MAS NMR spectra of the PV-1 catalyst are obtained and no decavanadate (at δ_{51V} = -430 and −510 ppm) could be detected, which suggests that the formed $AlVO_4$ clusters or Al-O-V linkages are highly stable. This is attributed to the strong interaction between surface defects and VO_4^{3-}, which inhibits the polymerization of VO_4^{3-} to regenerate decavanadates and crystal V_2O_5 species upon rehydration, in contrast to the often observed behavior of sol–gel prepared V/Al_2O_3 catalysts (V surface density > 8 V/nm^2) [25–28].

The proposed structure of the dominant VO_x species on the dehydrated SSV and PV catalysts is drawn in Fig. 9. The existence of decavanadates in the local structure of Al^{V} has been observed in Fig. 7. Decavanadates decomposition results in single-site,

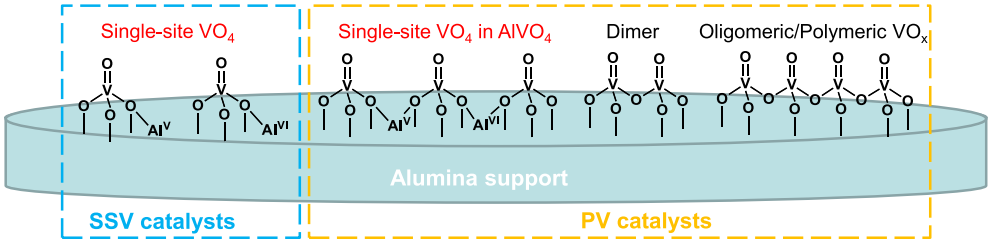


Fig. 9. Possible structures of dominant VO_x species on FSP-made V/Al_2O_3 catalysts. The proposed dominant active VO_x species are highlighted in red.

Table 5
Chemical shift parameters of the dehydrated V/Al_2O_3 catalysts.

Hydrated sample	Chemical shift δ_{iso} [a] (ppm)	C_{QCC} MHz	η	Concentration (%)
PV-2	−11 ($AlVO_4$)	1.8	0.25	21.8
	12 ($AlVO_4$)	6.0	0.55	9.6
	33 ($AlVO_4$)	6.8	0.42	6.7
	57 (Al^{IV})		0.5	13.1
	35 (Al^{V})		0.5	22.1
	10 (Al^{VI})		0.5	26.7
PV-1	−9 ($AlVO_4$)	1.8	0.25	6.8
	11 ($AlVO_4$)	6.0	0.55	10.3
	34 ($AlVO_4$)	6.8	0.45	9.8
	58 (Al^{IV})		0.5	16.2
	35 (Al^{V})		0.5	22.8
	9 (Al^{VI})		0.5	34.2
SSV	13 (Al^{VI}—VO_4)	6.0	0.6	11.1
	28 (Al^{V}—VO_4)	6.8	0.42	17.9
	58 (Al^{IV})		0.5	17.4
	35 (Al^{V})		0.5	18.1
	8 (Al^{VI})		0.5	35.5

[a] Isotropic chemical shifts (δ_{iso}), quadrupole coupling constant (C_{QCC}), and asymmetry parameters of the electric field gradient tensor (η) of each aluminum species, determined by simulation of ^{27}Al MAS NMR spectra of the dehydrated V/Al_2O_3 catalysts.

dimeric, and oligomeric VO_x species, and the regeneration of decavanadates is unfavorable upon rehydration (Fig. S5). In terms of the rich (33–39%) surface defect sites (e.g. Al^{V}) in FSP-made V/Al_2O_3 catalysts, the small VO_x species are proposed to be stabilized at surface defect sites via Al-O-V linkages. Then, the small VO_x species undergo rearrangements to form crystalline $AlVO_4$ clusters in the PV catalysts as shown in Fig. 9, similar to those observed in $AlVO_4$ (via tri-coordinated oxygens). The formation of $AlVO_4$ species other than crystals species are in line with the $AlVO_4$ spceis can be observed in HRTEM images and NMR spectra but not in the corresponding XRD patterns. In terms of the rich surface defect sites (e.g. Al^{V}) in FSP-made V/Al_2O_3 catalysts, the small V species are proposed to be stabilized at surface defect sites via Al-O-V linkages, similar to those observed in $AlVO_4$ (via tri-coordinated oxygens), as shown in Fig. 9. The SSV catalyst lacks a crystalline $AlVO_4$ structure but exhibits similar Al-O-V linkages in the ^{51}V and ^{27}Al MAS NMR spectra (Figs. 6 and 8). Al^{V}-O-V (δ_{27Al} = 31 ppm) and Al^{VI}-O-V (δ_{27Al} = 13 ppm) species are dominant in the SSV catalyst (Table 5). Therefore, VO_4 species are proposed to be highly dispersed via coordination to surface Al defects (e.g. Al^{V}) through tri-coordinated oxygens. Nearly no tetrahedral VO_4 species (δ_{51V} = -690 and −727 ± 5 ppm) in polymeric vanadates could be observed (Fig. 6). Crystalline $AlVO_4$ is also observed in the CV-1 catalyst but the polymeric VO_4 species are dominant in the CV catalysts due to their high content and surface density of V.

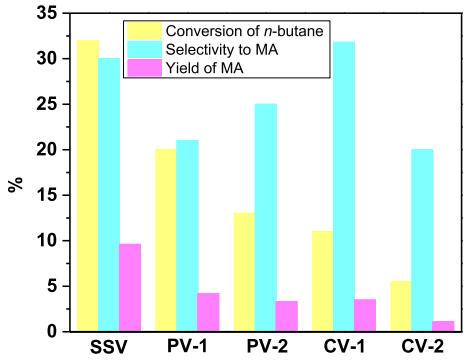


Fig. 10. Catalytic results of selective oxidation of MA over the V/Al_2O_3 catalysts with different V structures. Conditions: the reaction was performed at 623 K for 15 h with 1.5% *n*-butane (0.3 mL/min) and syn. Air (19.7 mL/min) at a total gas flow rate of 20 mL/min under atmospheric pressure.

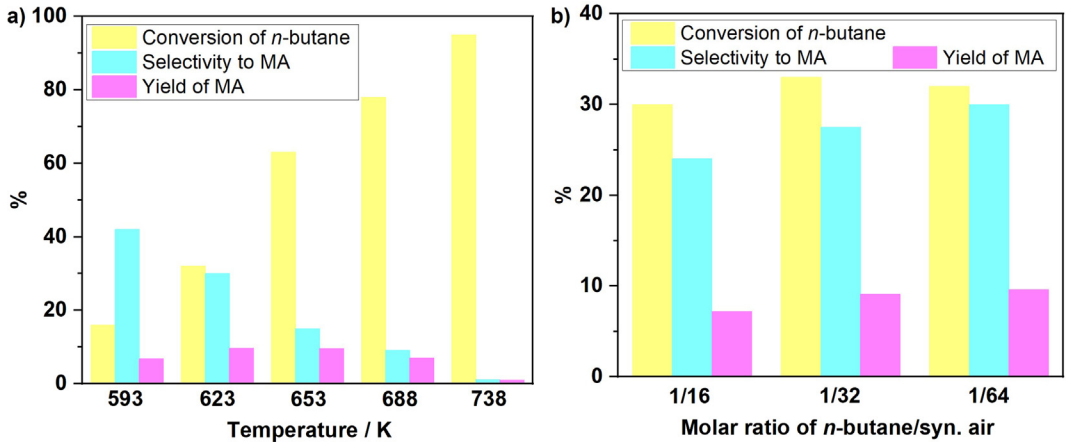


Fig. 11. Catalytic results of *n*-butane oxidation over the SSV catalyst: (a) as a function of different reaction temperatures. Conditions: 1.5% *n*-butane (0.3 mL/min) and syn. air (19.7 mL/min) under a total gas flow rate of 20 mL/min; (b) as a function of the molar ratio of *n*-butane/syn. air. Conditions: *n*-butane (0.3 mL/min) mixed with syn. air flow rate (4.5, 9.9, and 19.7 mL/min, and the gas mixture was balanced by N_2 to keep a constant total flow rate of 20 mL/min. The reaction was performed at 623 K.

3.2. Selective oxidation of n-butane over V/Al_2O_3 catalysts

The catalytic performances of all V/Al_2O_3 catalysts are summarized in Fig. 10. The conversion of *n*-butane strongly decreased from 32% for the SSV catalyst to 5.5% for the CV catalysts with increasing V content. The SSV and CV-1 catalysts exhibited similar selectivities to MA (30–32%), while the PV and CV-2 catalysts provided selectivities to MA of 20–25%, and thus, no clear dependence of the MA selectivity on the V content could be observed. However, a significant trend was observed for the yield of MA. The highest MA yield was obtained with the SSV catalyst. The PV and CV-1 catalysts offered lower than half of the MA yield of the SSV catalyst. The lowest *n*-butane conversion and yield of MA (1.1 %) were obtained with CV-2 (pure vanadium oxide). The high activity of the SSV catalyst is further confirmed by studying the V-atom efficiency of the V/Al_2O_3 catalysts (**Fig. S6**), which was evaluated by turnover frequencies (TOFs) calculated per V atoms for the conversion of *n*-butane producing MA. The highest TOFs were observed with the SSV catalyst, which are ca. 3–4 times higher than those obtained with the PV catalysts, and lower by a factor of ca. 20–100 for the CV catalysts.

Further, the effects of reaction temperature and *n*-butane/air ratio, and the gas flow rate on the performance of the SSV catalyst were investigated. As shown in Fig. 11**a**, the conversion of *n*-butane strongly depended on the reaction temperature, increasing from 11% to 96% with increasing temperature from 593 to 733 K. In contrast to *n*-butane conversion, the selectivity to MA was inversely proportional to the reaction temperature, decreasing from 42% to 1.9 %. The decrease of MA selectivity with increasing reaction temperature is caused by over oxidation of *n*-butane to carbon oxides at high temperature, a behavior reported for titania-supported vanadia catalysts [25]. The effect of the molar ratio of *n*-butane/syn. Air at a constant gas flow rate of 20 mL/min and *n*-butane flow rate of 0.3 mL/min is shown in Fig. 9**b**. The conversion of *n*-butane (30–33%) seems to be independent of the molar ratio, while the selectivity to MA strongly increased from 24% to 31% when reducing the molar ratio from 1/16 to 1/64. Under the current reaction temperature and without oxygen, a complete reduction of surface vanadia species on V/Al_2O_3 by *n*-butane has been reported [16]. The adequate oxygen concentration at a lower molar ratio of *n*-butane/syn. air could facilitate the regeneration of surface vanadia species, thereby promoting the oxidation of butane to MA.

The SSV catalyst shows excellent performance compared to those reported in the literature. As reported earlier [16], a MA yield of 3.2 % was obtained from the selective oxidation of *n*-butane (1.2 vol% *n*-butane with air at a total flow rate of 20 mL/min) with 17.5 wt% V_2O_5/Al_2O_3 (10.5 at.% V) at 494 K. With similar V content and 12.5 times higher *n*-butane to V ratio, the SSV catalyst provides ca. 3 times higher yield of MA under similar conditions but higher reaction temperature (623 K *vs*. 494 K) than the 17.5 wt% V_2O_5/Al_2O_3 catalyst. More significantly, the SSV catalyst affords 144 and 94 times higher TOFs of the *n*-butane conversion to MA than those obtained with 17.5 wt% V_2O_5/Al_2O_3, respectively. A clear difference is that the SSV species are the major sites on the SSV catalyst, while the polymeric vanadia species are dominant on the surface of the 17.5 wt% V_2O_5/Al_2O_3 catalyst.

As the best catalyst, the stability of the SSV catalyst was tested as shown in **Fig. S7**. Both similar *n*-butane conversion and selectivity to MA were achieved with the fresh and regenerated SSV catalyst at steady-state, which demonstrates its high stability. In addition, a significantly higher conversion but lower selectivity was observed at the initial state, which is attributed to the oxygen-rich surface caused by *in situ* catalyst activation in air.

The structure–activity relationship of V/Al_2O_3 catalysts was studied to understand the excellent performance of the SSV catalyst. Based on the structural characterization, surface vanadia species, including SSV species, polymeric VO_x species, bulk-like V_2O_5, and $AlVO_4$, could exist on the surface of V/Al_2O_3 catalysts. The terminal V = O and V-O-V are dominant functionalities on CV catalysts. A previous theoretical study revealed that the V = O groups on crystalline V_2O_5 are quite stable for catalytic reactions [50]. The bridging V–O–V bonds are formed by the polymerization of VO_x species on V/Al_2O_3 catalysts. The oxygens in the bridging V–O–V bonds are suggested to be virtually inactive in the oxidation reaction [68,69]. These reports well explain the poor activity of CV catalysts observed here. Both SSV and PV catalysts are dominantly populated with single-site VO_4 species, which are often considered key active sites for the conversion of *n*-butane to MA. $AlVO_4$ clusters are the most abundant VO_4 species on the PV catalysts. $AlVO_4$ contains isolated VO_4^{3-} units, AlO_4 tetrahedra, and AlO_6 octahedra as evidenced by IR, XRD, and theoretical studies [70–72]. Since no V-O-V bond could be formed, the tetrahedral VO_4^{3-} species in $AlVO_4$ clusters are isolated, which are also SSV but in the vicinity of the PV catalysts as shown in Fig. 9. Compared to the $AlVO_4$ clusters on the PV catalysts, the VO_4 species on the SSV catalyst are highly separated and stabilized by neighboring Al defects. The best performance of the SSV catalyst disqualifies the isolated VO_4 in the $AlVO_4$ clusters from being the most relevant catalytic sites in FSP V/Al_2O_3 catalysts.

The reaction mechanism based on supported VO_x catalysts is rarely reported in the literature, except for VPO catalysts. Several surface V sites on VPO catalysts, such as the V^{5+}/V^{4+} redox couple, are proposed to promote MA formation via the alkene route or the alkoxide route [9,10]. The quantitative analysis of supported VPO catalysts using solid-state NMR spectroscopy suggested the key role of tetrahedral V^{5+}=O species in this reaction [6,11]. A single-site organometallic mechanism is proposed for the selective oxidation of *n*-butane at V = O sites on VPO catalysts based on ^{13}C MAS NMR studies of the reaction [8]. Based on this reaction mechanism, the activated *n*-butane rearranges to coordinate with a vanadium ion via C1 and C4 of butane, which is maintained for the insertion of three oxygen atoms and abstraction of eight hydrogen atoms, until the formation of MA. This is similar to those proposed for the catalytic oxidation of hydrocarbons on vanadium oxides through a Mars-Van Krevelen mechanism [18]. The general Mars-Van Krevelen mechanism promoting selective oxidation reaction comprises the following steps: (i) a lattice oxygen atom is transferred to the activated reactant molecule leaving a surface oxygen vacancy; (ii) then a gas-phase O_2 is adsorbed at the oxygen vacancy site, and (iii) the adsorbed O_2 contributes one oxygen atom to the activated reactant and one to rearrange the surface structure. The Mars-Van Krevelen mechanism has been recently confirmed by DFT calculations of CO oxidation over V-doped CeO_2 catalysts [73].

The SSV catalyst showing the best performance among V/Al_2O_3 catalysts allows us to assign SSV species as the active sites in the

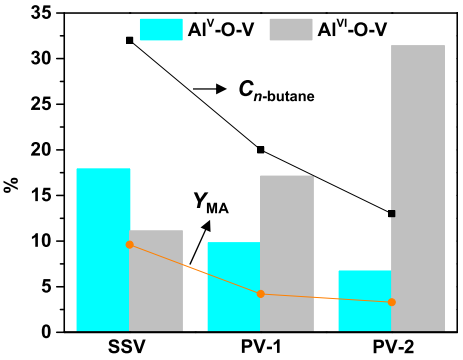
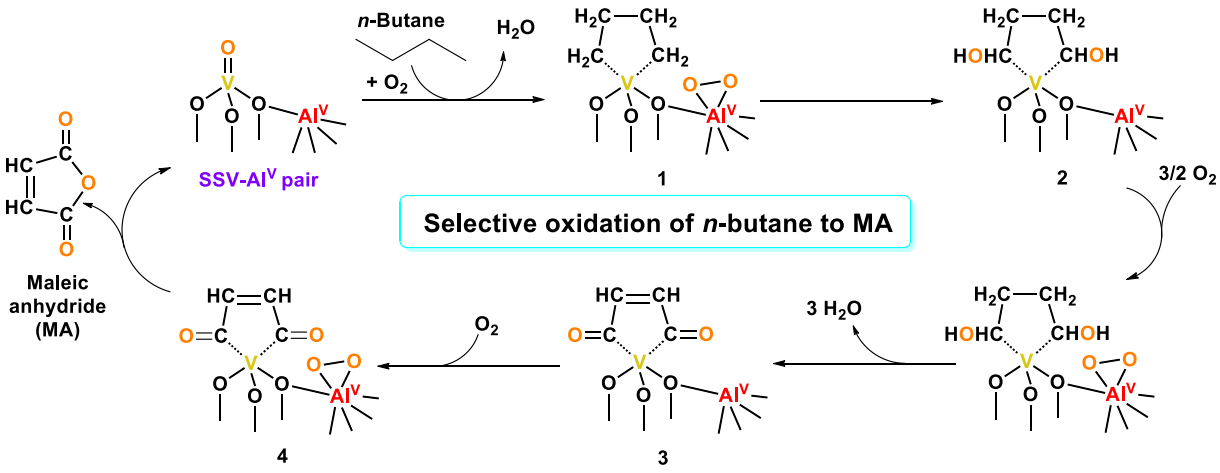


Fig. 12. Catalytic results of the selective oxidation of MA over the V/Al_2O_3 catalysts depending on their population with Al-O-V species.



Scheme 2. Proposed reaction mechanism for selective oxidation of *n*-butane to MA through cooperative action of SSV-Al^V pairs on the SSV catalysts.

selective conversion of *n*-butane to MA. The adsorption of oxygen on the alumina surface has been reported for a long time [74]. Al^V species are the major defect sites on alumina and are identified as Al^{VI} with an oxygen vacancy [75]. Therefore, the strong Lewis acidic Al^V sites could act as oxygen vacancy sites to adsorb molecular oxygen. The adsorption of oxygen molecules at Al^V sites (oxygen vacancy on Al(1 1 1)) has been confirmed recently by DFT calculations, which showed that the O_2 could be dissociated into oxygen atoms and diffuse on the surface depending on the local environment [76]. As shown in Fig. 9, the SSV species are located in the vicinity of Al^V and/or Al^V species. Therefore, the catalytic performances of the SSV and PV catalysts as a function of Al^V or Al^V species nearby are shown in Fig. 12. The *n*-butane conversion was enhanced with the increase of the Al^V-O-V linkages (single-site VO_4 and Al^V pairs), but inverse to the significant decrease of the Al^{VI}-O-V linkages (single-site VO_4 and Al^{VI} pairs). The Al^V sites could adsorb and activate oxygen to promote butane oxidation at neighboring SSV species on the SSV catalyst, which is difficult on the saturated Al^{VI} sites. However, this cooperative action is hindered by the structure of $AlVO_4$ in PV catalysts, reducing the MA selectivity. For CV catalysts, both the concentrations of single-site VO_4 species and Al^V species are rapidly reduced with increasing V content, leading to a strong decrease in catalytic performance.

The relationship between MA yield and various V-O sites, e.g. Al^V-O-V, Al^{VI}-O-V, V = O, V-O-V, was investigated to confirm the active sites on V/Al_2O_3. As shown in Fig. 10, CV-2 (pure vanadium oxide) having mainly V-O-V and terminal V = O sites is inactive with the lowest yield of MA (1.1 %). The highest MA yield was obtained with the SSV catalyst, while the PV and CV-1 catalysts afforded medium MA yields, only half of that obtained with the SSV catalyst. SSV-Al pairs are prevalent on the SSV catalyst, while the PV and CV-1 catalysts consist of mainly $AlVO_4$ and V_2O_5. Therefore, the key sites in the transformation of *n*-butane to MA are the SSV-Al pairs. Fig. 12 demonstrate that the MA yield increased with increasing the Al^V-O-V linkages but not with the Al^{VI}-O-V linkages in the SSV-Al pairs. Therefore, the reaction mechanism based on the SSV-Al pairs was further investigated.

The formation of strong SSV-Al pairs in the SSV catalysts has been supported by the significant ^{51}V chemical shift observed with the SSV and PV catalysts. $AlVO_4$ peaks shift to high frequency from δ_{51V} = -727 and −785 ppm for the PV-2 catalyst to δ_{51V} = -723 and −780 ppm for the PV-1 catalyst. This shift is more significant with the broad peaks towards high frequency (at δ_{51V} = -644 and −764 ppm) for the SSV catalyst, which is attributed to the significant deshielding of ^{51}V resonance. The deshielding hints at a longer average V-O distance or weaker V-O interaction, demonstrating a stronger electron-withdrawing effect of Al sites on the neighboring V atom via the Al-O-V linkage on the SSV catalysts. A longer V-O distance is often reported to facilitate oxygen releasing and enhance the activity of supported VO_x species in oxidation reactions. For instance, the longer V-O distance of single-site VO_4 species on VO_x/SiO_2 than on VO_x/Al_2O_3 catalysts provides a higher conversion but a lower selectivity in oxidative dehydrogenation (ODH) of propane to propene [77,78]. The higher conversion obtained with the SSV catalyst correlates well with the longer V-O distance compared to that in the PV catalysts. On the other hand, the shorter V-O distance may hinder oxygen release from the PV catalysts, which could impede MA from overoxidation, corresponding to the high MA selectivity obtained with the PV-2 catalyst compared to the PV-1 catalyst. However, the SSV catalyst provides a much higher MA selectivity than the PV catalysts. In terms of the steric effects and the vicinity of VO_4 sites in the $AlVO_4$ cluster, the activation of oxygen on the Al^V sites is less favorable. Therefore, a reaction mechanism for the *n*-butane oxidation to MA has been proposed with the cooperativity of two neighboring VO_4 sites in the $AlVO_4$ cluster (**Scheme S1**). Adsorption of O_2 at the defects on alumina results in a bond length (1.49 Å) shorter than the V = O bond length (1.59 Å) [70,77], which could be the reason for the higher selectivity obtained on the SSV catalyst than on the PV catalysts.

Here, we propose a reaction mechanism for the selective oxidation of *n*-butane to MA at single-site VO_4 sites associated with nearby Al^V species, defined as SSV-Al^V pairs on the SSV catalyst. As shown in Scheme 2, (1) the *n*-butane is firstly activated with the cleavage of methylene carbon-hydrogen bonds at the surface V = O of VO_4 sites, similar to the single-site organometallic mechanism [79]; (2) the activated *n*-butane rearranges to coordinate with a vanadium ion via C1 and C4 of *n*-butane (1); (3) oxygen insertion with O_2 captured by a neighboring Al^V site as an oxygen vacancy site (2 and 3); (4) the release of Al^V site as oxygen vacancy and O_2 re-adsorption; and (5) the desorption of MA (4). This mechanism can well explain the high activity of SSV catalysts.

4. Conclusion

In this work, V/Al_2O_3 catalysts with various V/Al ratios have been developed for the selective oxidation of *n*-butane to MA. The existence of single-site VO_4 (SSV), polymeric VO_4 species, crystalline $AlVO_4$ clusters, nanoparticles, and crystals was identified using ^{51}V and ^{27}Al solid-state NMR spectroscopy and confirmed by XRD, HRTEM, Raman, and UV–vis spectroscopies. Terminal

V = O and V-O-V functionalities on the nanoparticles and crystals of vanadium oxide as well as the isolated VO_4 sites in the $AlVO_4$ clusters exhibit relatively low activity in the conversion of *n*-butane to MA as demonstrated by their poor MA yield. The catalyst (V/Al = 1/9) having mainly SSV provides a more than two times higher MA yield than the other V/Al_2O_3 catalysts.

In the SSV catalyst, the single-site VO_x species are highly isolated on the surface and stabilized by neighboring Al defect sites, such as Al^V sites. Molecular oxygens can be activated at surface Al^V sites and then react with the activated *n*-butane at SSV sites to yield MA. In contrast, the steric effects and the vicinity of VO_4 sites in the $AlVO_4$ clusters leading to the activation of oxygen on the Al^V sites are less favorable. Instead, the oxidation of *n*-butane is proposed to occur by the cooperative action of two neighboring VO_4 sites in the $AlVO_4$ cluster. Therefore, the SSV-Al^V pairs have been identified as the key sites promoting the selective oxidation of *n*-butane to MA and a corresponding reaction mechanism is proposed in Scheme 2. This work likely provides the most active supported V catalysts for the selective oxidation of *n*-butane to MA reported so far in the literature, apart from the well-known VPO catalysts. It also sheds new light on promoting the catalytic activity through the cooperative action of SSV and other functional groups (e.g. Al^V) nearby as an alternative to the SSV-only based catalysis.

Declaration of Competing Interest

The authors declare that they have no known competing financial interests or personal relationships that could have appeared to influence the work reported in this paper.

Acknowledgements

This work was supported by the Australian Research Council Discovery Projects (DP150103842 and DE190101618), the SOAR Fellowship, and the Sydney Nano Grand Challenge from the University of Sydney.

Appendix A. Supplementary material

Supplementary data to this article can be found online at https://doi.org/10.1016/j.jcat.2022.06.013.

References

[1] T.R. Felthouse, J.C. Burnett, B. Horrell, M.J. Mummey, Y.-J. Kuo, Maleic Anhydride, Maleic Acid, and Fumaric Acid, in: Kirk-Othmer Encyclopedia of Chemical Technology, John Wiley & Sons, Inc., Hoboken, NJ, 2001, pp. 1-49.
[2] J.H. Teles, I. Hermans, G. Franz, R.A. Sheldon, Oxidation, in: Ullmann's Encyclopedia of Industrial Chemistry, Wiley, 2015, pp. 1-103.
[3] H.-M. Zhang, Q.-Y. Fan, Q.-H. Zhang, J.-C. Kang, Y.e. Wang, J. Cheng, Understanding catalytic mechanisms of alkane oxychlorination from the perspective of energy levels, J. Phys. Chem. C 124 (11) (2020) 6070–6077.
[4] R.L. Bergman, and N.W. Frisch, Production of maleic anhydride by oxidation of *n*-butane, US Patent 3293268 (1966).
[5] Z. Xie, B. Chen, L. Zheng, F. Peng, H. Liu, B. Han, Monomeric vanadium oxide: a very efficient species for promoting aerobic oxidative dehydrogenation of N-heterocycles, New J. Chem. 45 (2021) 431–437.
[6] J. Frey, C. Lieder, T. Schölkopf, T. Schleid, U. Nieken, E. Klemm, M. Hunger, Quantitative solid-state NMR investigation of V^{5+} species in VPO catalysts upon sequential selective oxidation of n-butane, J. Catal. 272 (1) (2010) 131–139.
[7] C. Hess, Nanostructured vanadium oxide model catalysts for selective oxidation reactions, ChemPhysChem 10 (2) (2009) 319–326.
[8] B. Chen, E.J. Munson, Investigation of the mechanism of *n*-butane oxidation on vanadium phosphorus oxide catalysts: Evidence from isotopic labeling studies, J. Am. Chem. Soc. 124 (2002) 1638–1652.
[9] Y. Zhanglin, M. Forissier, R.P. Sneeden, J.C. Vedrine, J.C. Volta, On the mechanism of *n*-butane oxidation to maleic-anhydride on VPO catalysts. 1. A kinetics study on a VPO catalyst as compared to VPO reference phases, J. Catal. 145 (2) (1994) 256–266.
[10] G. Centi, F. Trifiro, J.R. Ebner, V.M. Franchetti, Mechanistic aspects of maleic anhydride synthesis from C4 hydrocarbons over phosphorus vanadium oxide, Chem. Rev. 88 (1) (1988) 55–80.
[11] J. Frey, Y. Sang Ooi, B. Thomas, V.R. Reddy Marthala, A. Bressel, T. Schölkopf, T. Schleid, M. Hunger, Vanadium phosphates on mesoporous supports: model catalysts for solid-state NMR studies of the selective oxidation of *n*-butane, Solid State Nucl, Magn. Reson. 35 (2009) 130–137.
[12] G.J. Hutchings, A. Desmartin-Chomel, R. Olier, J.-C. Volta, Role of the product in the transformation of a catalyst to its active state, Nature 368 (6466) (1994) 41–45.
[13] G.J. Hutchings, J.A. Lopez-Sanchez, J.K. Bartley, J.M. Webster, A. Burrows, C.J. Kiely, A.F. Carley, C. Rhodes, M. Hävecker, A. Knop-Gericke, R.W. Mayer, R. Schlögl, J.C. Volta, M. Poliakoff, Amorphous vanadium phosphate catalysts prepared using precipitation with supercritical CO_2 as an antisolvent, J. Catal. 208 (1) (2002) 197–210.
[14] I.E. Wachs, J.-M. Jehng, G. Deo, B.M. Weckhuysen, V.V. Guliants, J.B. Benziger, In situ Raman spectroscopy studies of bulk and surface metal oxide phases during oxidation reactions, Catal. Today 32 (1-4) (1996) 47–55.
[15] V.V. Guliants, Structure–reactivity relationships in oxidation of C4 hydrocarbons on supported vanadia catalysts, Catal. Today 51 (1999) 255–268.
[16] I.E. Wachs, J.-M. Jehng, G. Deo, B.M. Weckhuysen, V.V. Guliants, J.B. Benziger, S. Sundaresan, Fundamental studies of butane oxidation over model-supported vanadium oxide catalysts: Molecular structure-reactivity relationships, J. Catal. 170 (1997) 75–88.
[17] T. Kim, I.E. Wachs, CH_3OH oxidation over well-defined supported V_2O_5/Al_2O_3 catalysts: Influence of vanadium oxide loading and surface vanadium-oxygen functionalities, J. Catal. 255 (2008) 197–205.
[18] P. Mars, D.W. van Krevelen, Oxidations carried out by means of vanadium oxide catalysts, Chem. Eng. Sci. 3 (1954) 41–59.
[19] R. Koirala, S.E. Pratsinis, A. Baiker, Synthesis of catalytic materials in flames: opportunities and challenges, Chem. Soc. Rev. 45 (2016) 3053–3068.
[20] R. Mueller, L. Mädler, S.E. Pratsinis, Nanoparticle synthesis at high production rates by flame spray pyrolysis, Chem. Eng. Sci. 58 (10) (2003) 1969–1976.
[21] Z. Wang, Y. Jiang, A. Baiker, J. Huang, Pentacoordinated aluminum species: New frontier for tailoring acidity-enhanced silica–alumina catalysts, Acc. Chem. Res. 53 (2020) 2648–2658.
[22] Z. Wang, Y. Jiang, X. Yi, C. Zhou, A. Rawal, J. Hook, Z. Liu, F. Deng, A. Zheng, M. Hunger, A. Baiker, J. Huang, High population and dispersion of pentacoordinated Al^V species on the surface of flame-made amorphous silica-alumina, Sci. Bull. 64 (8) (2019) 516–523.
[23] Z. Wang, K. Chen, Y. Jiang, J. Trébosc, W. Yang, J.-P. Amoureux, I. Hung, Z. Gan, A. Baiker, O. Lafon, J. Huang, Revealing Brønsted acidic bridging SiOHAl groups on amorphous silica–alumina by ultrahigh field solid-state NMR, J. Phys. Chem. Lett. 12 (47) (2021) 11563–11572.
[24] Z. Wang, T. Li, Y. Jiang, O. Lafon, Z. Liu, J. Trébosc, A. Baiker, J.-P. Amoureux, J. Huang, Acidity enhancement through synergy of penta- and tetra-coordinated aluminum species in amorphous silica networks, Nat. Commun. 11 (2020) 225.
[25] I.E. Wachs, B.M. Weckhuysen, Structure and reactivity of surface vanadium oxide species on oxide supports, Appl. Catal. A: Gen. 157 (1997) 67–90.
[26] A. Khodakov, B. Olthof, A.T. Bell, E. Iglesia, Structure and catalytic properties of supported vanadium oxides: Support effects on oxidative dehydrogenation reactions, J. Catal. 181 (1999) 205–216.
[27] D.E. Keller, T. Visser, F. Soulimani, D.C. Koningsberger, B.M. Weckhuysen, Hydration effects on the molecular structure of silica-supported vanadium oxide catalysts: A combined IR, Raman, UV–vis and EXAFS study, Vib. Spectrosc. 43 (2007) 140–151.
[28] B. Grzybowska-Świerkosz, Vanadia-titania catalysts for oxidation of o-xylene and other hydrocarbons, Appl. Catal. A: Gen. 157 (1997) 263–310.
[29] R. Strobel, S.E. Pratsinis, Flame aerosol synthesis of smart nanostructured materials, J. Mater. Chem. 17 (2007) 4743–4756.
[30] Z. Wang, Y. Jiang, F. Jin, C. Stampfl, M. Hunger, A. Baiker, J. Huang, Strongly enhanced acidity and activity of amorphous silica–alumina by formation of pentacoordinated Al^V species, J. Catal. 372 (2019) 1–7.
[31] R. Dwivedi, P. Sharma, A. Sisodiya, M.S. Batra, R. Prasad, A DFT-assisted mechanism for evolution of the ammoxidation of 2-chlorotoluene (2-CLT) to 2-chlorobenzonitrile (2-CLBN) over alumina-supported V_2O_5 catalyst prepared by a solution combustion method, J. Catal. 345 (2017) 245–257.
[32] E. Reddy, Preparation, characterization, and activity of Al_2O_3-supported V_2O_5 catalysts, J. Catal. 221 (1) (2004) 93–101.
[33] B, Hari Babu, K.T, Venkateswara Rao, Y.W, Suh, P.S, Sai Prasad, N, Lingaiah, One-step selective synthesis of 2-chlorobenzonitrile from 2-chlorotoluene via ammoxidation, New J. Chem. 42 (2018) 1892–1901.
[34] M.Z. Wu, X.F. Zhang, S. Gao, X.L. Cheng, Z.M. Rong, Y.M. Xu, H. Zhao, L.H. Huo, Construction of monodisperse vanadium pentoxide hollow spheres via a facile route and triethylamine sensing property, CrystEngComm 15 (2013) 10123–10131.
[35] Y.P. Chen, G. Yang, Z.H. Zhang, X.Y. Yang, W.H. Hou, J.J. Zhu, Polyaniline-intercalated layered vanadium oxide nanocomposites-one-pot hydrothermal synthesis and application in lithium battery, Nanoscale 2 (2010) 2131–2138.
[36] L.K. Boudali, A. Ghorbel, P. Grange, F. Figueras, Selective catalytic reduction of NO with ammonia over V_2O_5 supported sulfated titanium-pillared clay catalysts: influence of V_2O_5 content, Appl. Catal. B: Environ. 59 (1-2) (2005) 105–111.

[37] B. Schimmoeller, S.E. Pratsinis, A. Baiker, Flame aerosol synthesis of metal oxide catalysts with unprecedented structural and catalytic properties, ChemCatChem 3 (8) (2011) 1234–1256.
[38] W.Y. Teoh, R. Amal, L. Maedler, Flame spray pyrolysis: An enabling technology for nanoparticles design and fabrication, Nanoscale 2 (2010) 1324–1347.
[39] J. Huang, N. van Vegten, Y. Jiang, M. Hunger, A. Baiker, Increasing the Brønsted acidity of flame-derived silica/alumina up to zeolitic strength, Angew. Chem. Int. Ed. 49 (42) (2010) 7776–7781.
[40] J.G. Eon, R. Olier, J.C. Volta, Oxidative dehydrogenation of propane on γ-Al_2O_3 supported vanadium oxides, J. Catal. 145 (2) (1994) 318–326.
[41] T. Blasco, A. Galli, J.M. López Nieto, F. Trifiró, Oxidative dehydrogenation of ethane and *n*-butane on VO_x/Al_2O_3 Catalysts, J. Catal. 169 (1) (1997) 203–211.
[42] M. Baltes, K. Cassiers, P. Van Der Voort, B.M. Weckhuysen, R.A. Schoonheydt, E. F. Vansant, MCM-48-supported vanadium oxide catalysts, prepared by the molecular designed dispersion of $VO(acac)_2$: A detailed study of the highly reactive MCM-48 surface and the structure and activity of the deposited VO_x, J. Catal. 197 (2001) 160–171.
[43] H. Berndt, A. Martin, A. Brückner, E. Schreier, D. Müller, H. Kosslick, G.-U. Wolf, B. Lücke, Structure and catalytic properties of VO_x/MCM materials for the partial oxidation of methane to formaldehyde, J. Catal. 191 (2) (2000) 384–400.
[44] A. Qiao, V.N. Kalevaru, J. Radnik, A. Duvel, P. Heitjans, A.S.H. Kumar, P.S.S. Prasad, N. Lingaiah, A. Martin, Oxidative dehydrogenation of ethane to ethylene over V_2O_5/Al_2O_3 catalysts: Effect of source of alumina on the catalytic performance, Ind. Eng. Chem. Res. 53 (2014) 18711–18721.
[45] X. Gao, S.R. Bare, J.L.G. Fierro, I.E. Wachs, Structural characteristics and reactivity/reducibility properties of dispersed and bilayered $V_2O_5/TiO_2/SiO_2$ catalysts, J. Phys. Chem. B 103 (4) (1999) 618–629.
[46] M. Fournier, C. Louis, M. Che, P. Chaquin, D. Masure, Polyoxometallates as models for oxide catalysts: Part I. An UV-visible reflectance study of polyoxomolybdates: Influence of polyhedra arrangement on the electronic transitions and comparison with supported molybdenum catalysts, J. Catal. 119 (1989) 400–414.
[47] D. Masure, P. Chaquin, C. Louis, M. Che, M. Fournier, Polyoxometallates as models for oxide catalysts: Part II. Theoretical semi-empirical approach to the influence of the inner and outer Mo coordination spheres on the electronic levels of polyoxomolybdates, J. Catal. 119 (1989) 415–425.
[48] G. Busca, L. Marchetti, G. Centi, F. Trifirò, Surface characterization of a grafted vanadium–titanium dioxide catalyst, J. Chem. Soc. Faraday Trans. 1: Physical Chemistry in Condensed Phases 81 (1985) 1003.
[49] L. Owens, H.H. Kung, The effect of loading of vanadia on silica in the oxidation of butane, J. Catal. 144 (1) (1993) 202–213.
[50] N. Magg, B. Immaraporn, J. BGiorgi, T. Schroeder, M. Bäumer, J. Döbler, Z. Wu, E. Kondratenko, M. Cherian, M. Baerns, P.C. Stair, J. Sauer, H.-J. Freund, Vibrational spectra of alumina- and silica-supported vanadia revisited: An experimental and theoretical model catalyst study, J. Catal. 226 (2004) 88–100.
[51] B. Olthof, A. Khodakov, A.T. Bell, E. Iglesia, Effects of support composition and pretreatment conditions on the structure of vanadia dispersed on SiO_2, Al_2O_3, TiO_2, ZrO_2, and HfO_2, J. Phys. Chem. B 104 (7) (2000) 1516–1528.
[52] M.D. Argyle, K. Chen, C. Resini, C. Krebs, A.T. Bell, E. Iglesia, Extent of reduction of vanadium oxides during catalytic oxidation of alkanes measured by in-situ UV−visible spectroscopy, J. Phys. Chem. B 108 (7) (2004) 2345–2353.
[53] G.T. Went, S.T. Oyama, A.T. Bell, Laser Raman spectroscopy of supported vanadium oxide catalysts, J. Phys. Chem. 94 (10) (1990) 4240–4246.
[54] J. Döbler, M. Pritzsche, J. Sauer, Oxidation of methanol to formaldehyde on supported vanadium oxide catalysts compared to gas phase molecules, J. Am. Chem. Soc. 127 (31) (2005) 10861–10868.
[55] A.E. Lewandowska, M.A. Bañares, D.F. Khabibulin, O.B. Lapina, Precursor effect on the molecular structure, reactivity, and stability of alumina-supported vanadia, J. Phys. Chem. C 113 (2009) 20648–20656.
[56] N. Shiju, M. Anilkumar, S. Mirajkar, C. Gopinath, B. Rao, C. Satyanarayana, Oxidative dehydrogenation of ethylbenzene over vanadia-alumina catalysts in the presence of nitrous oxide: structure-activity relationship, J. Catal. 230 (2005) 484–492.
[57] O.B. Lapina, V.M. Mastikhin, L.G. Simonova, Y.O. Bulgakova, Characterization of surface species of supported V_2O_5/Al_2O_3 catalysts by ^{51}V NMR, J. Mol. Catal. 69 (1991) 61–73.
[58] U.G. Nielsen, A. Boisen, M. Brorson, C.J.H. Jacobsen, H.J. Jakobsen, J. Skibsted, Aluminum Orthovanadate ($AlVO_4$): Synthesis and characterization by ^{27}Al and ^{51}V MAS and MQMAS NMR spectroscopy, Inorg. Chem. 41 (2002) 6432–6439.
[59] H. Eckert, I.E. Wachs, Solid-state vanadium-51 NMR structural studies on supported vanadium(V) oxide catalysts: vanadium oxide surface layers on alumina and titania supports, J. Phys. Chem. 93 (1989) 6796–6805.
[60] J. McGregor, Z. Huang, G. Shiko, L.F. Gladden, R.S. Stein, M.J. Duer, Z. Wu, P.C. Stair, S. Rugmini, S.D. Jackson, The role of surface vanadia species in butane dehydrogenation over VO_x/Al_2O_3, Catal. Today 142 (3-4) (2009) 143–151.
[61] K.V. Bineesh, M.-I. Kim, G.-H. Lee, M. Selvaraj, D.-W. Park, Catalytic performance of vanadia-doped alumina-pillared clay for selective oxidation of H_2S, Appl. Clay Sci. 74 (2013) 127–134.
[62] M. Aureliano, C.A. Ohlin, M.O. Vieira, M.P.M. Marques, W.H. Casey, L.A.E. Batista De Carvalho, Characterization of decavanadate and decaniobate solutions by Raman spectroscopy, Dalton Trans. 45 (2016) 7391–7399.
[63] L. Ulická, L. Zúrková, Thermal reactivity of decavanadates, J. Thermal Analysis 20 (1981) 147–151.
[64] N.I. Gumerova, A. Rompel, Polyoxometalates in solution: speciation under spotlight, Chem. Soc. Rev. 49 (2020) 7568–7601.
[65] S. Ekambaram, K.C. Patil, Rapid synthesis and properties of $FeVO_4$, $AlVO_4$, YVO_4 and Eu^{3+}-doped YVO_4, J. Alloys Compd. 217 (1) (1995) 104–107.
[66] I.E. Wachs, Catalysis science of supported vanadium oxide catalysts, Dalton Trans. 42 (2013) 11762.
[67] T. Machej, J. Haber, A.M. Turek, I.E. Wachs, Monolayer V_2O_5/TiO_2 and MoO_3/TiO_2 catalysts prepared by different methods, Appl. Catal. 70 (1) (1991) 115–128.
[68] L.E. Briand, J.-M. Jehng, L. Cornaglia, A.M. Hirt, I.E. Wachs, Quantitative determination of the number of surface active sites and the turnover frequency for methanol oxidation over bulk metal vanadates, Catal. Today 78 (1-4) (2003) 257–268.
[69] I.E. Wachs, Molecular engineering of supported metal oxide catalysts: Oxidation reactions over supported vanadia catalysts, in: J.J. Spivey (Ed.), Catalysis, Volume 13, The Royal Society of Chemistry, 1997, pp. 37–54.
[70] V. Brázdová, M.V. Ganduglia-Pirovano, J. Sauer, Crystal structure and vibrational spectra of $AlVO_4$. A DFT Study, J. Phys. Chem. B 109 (1) (2005) 394–400.
[71] A.A. Coelho, Whole-profile structure solution from powder diffraction data using simulated annealing, J. Appl. Crystallogr. 33 (3) (2000) 899–908.
[72] O. Yamaguchi, T. Uegaki, Y. Miyata, K. Shimizu, Formation of $AlVO_4$ solid solution from alkoxides, J. Am. Ceram. Soc. 70 (8) (1987) C-198–C-200.
[73] .B. Liu, W. Li, W. Song, J. Liu, Carbonate-mediated Mars–van Krevelen mechanism for CO oxidation on cobalt-doped ceria catalysts: facet-dependence and coordination-dependence, Phys. Chem. Chem. Phys. 20 (2018) 16045–16059.
[74] L.N. Mulay, L.K. Keys, Studies on adsorption of oxygen on γ-alumina. Nature of adsorbed species, J. Am. Chem. Soc. 87 (1965) 1192–1195.
[75] K.J.D. MacKenzie, J. Temuujin, K. Okada, Thermal decomposition of mechanically activated gibbsite, Thermochimica Acta 327 (1-2) (1999) 103–108.
[76] M. Guiltat, M. Brut, S. Vizzini, A. Hémeryck, Dioxygen molecule adsorption and oxygen atom diffusion on clean and defective aluminum(111) surface using first principles calculations, Surf. Sci. 657 (2017) 79–89.
[77] I. Rossetti, G.F. Mancini, P. Ghigna, M. Scavini, M. Piumetti, B. Bonelli, F. Cavani, A. Comite, Spectroscopic enlightening of the local structure of VO_X active sites in catalysts for the ODH of propane, J. Phys. Chem. C 116 (42) (2012) 22386–22398.
[78] I. Rossetti, L. Fabbrini, N. Ballarini, C. Oliva, F. Cavani, A. Cericola, B. Bonelli, M. Piumetti, E. Garrone, H. Dyrbeck, E.A. Blekkan, L. Forni, V-Al–O catalysts prepared by flame pyrolysis for the oxidative dehydrogenation of propane to propylene, Catal. Today 141 (3-4) (2009) 271–281.
[79] M.A. Pepera, J.L. Callahan, M.J. Desmond, E.C. Milberger, P.R. Blum, N.J. Bremer, Fundamental study of the oxidation of butane over vanadyl pyrophosphate, J. Am. Chem. Soc. 107 (17) (1985) 4883–4892.